

# Cross-gyre transport by North Brazil Current rings

William E. Johns<sup>a\*</sup>, Rainer J. Zantopp<sup>a</sup>, and Gustavo J. Goni<sup>b</sup>

<sup>a</sup> Rosenstiel School of Marine and Atmospheric Science, University of Miami, 4600 Rickenbacker Causeway, Miami, Florida 33149, USA.

<sup>b</sup> National Oceanic and Atmospheric Administration, Atlantic Oceanographic and Meteorological Laboratory, Miami, Florida, USA.

Recent observations collected as part of the North Brazil Current Rings Experiment are used to assess the role played by NBC rings in tropical to subtropical cross-gyre transport in the Atlantic Ocean. During the course of the 20 month experiment, four different NBC Rings were surveyed by ships and twelve additional rings were identified by moored current meters and temperature/salinity recorders. Of the total of 16 rings observed, four were subsurface-intensified rings with little or no surface signal. Except for these subsurface rings, generally good agreement was found in the identification of NBC rings during the experiment by various techniques including satellite altimetry, ocean color, and inverted echo sounders. The observations of water properties in the ring cores provided by the *in-situ* temperature and salinity measurements are used to estimate the trapped core volumes of South Atlantic water in the rings. Based on these new measurements we estimate a ring formation rate of 8-9 rings per year, with no apparent seasonal variation in the formation rate. However, the surface rings show a seasonal cycle in their vertical penetration and associated trapped core volumes. Deeper rings tend to occur in fall and early winter, while shallower rings occur in spring and summer. The subsurface rings are usually smaller in diameter than the surface rings (average radius of maximum velocity 100 km versus 130 km), but have a thicker layer of trapped South Atlantic water and consequently a larger transport per ring. The average ring-induced transport including all ring types is about 1.1 Sv per ring, leading to an estimate of 9.3 Sv for the total annualized ring transport. This value is nearly twice that of most previous estimates, and suggests that NBC rings could account for more than half of the northward transport in the warm limb of the Atlantic meridional overturning cell.

---

\*Corresponding author: Tel.: +1-305-361-4054, Email: wjohns@rsmas.miami.edu

## 1. INTRODUCTION

The circulation in the western tropical Atlantic Ocean has a number of remarkable features, one of the most prominent being the seasonal retroflexion of the North Brazil Current into the North Equatorial Countercurrent near 6° N. It was discovered in the late 1980's that the North Brazil Current retroflexion oscillated about its mean location along the western boundary in a semi-periodic manner, and that in association with this variability it shed large anticyclonic rings that moved northwestward along the boundary (Johns *et al.*, 1990; Didden and Schott, 1993; Richardson *et al.*, 1994). Since this discovery it has been suggested by many authors that NBC rings could play an important role in the net meridional transport of warm waters in the upper layers of the Atlantic Ocean as part of the meridional overturning circulation (MOC).

A key issue in resolving the importance of the rings within the MOC is to quantify the amount of water of South Atlantic origin that they trap in their cores and carry with them into the North Atlantic. Early studies of NBC rings all suggested a similar amount of South Atlantic water transported by NBC rings, amounting to about 3 Sv on an annualized basis (Johns *et al.*, 1990; Didden and Schott; 1993, Richardson *et al.*, 1994; Fratantoni *et al.*, 1995). However, these estimates were based on different assumptions about the number of rings shed in each year as well as the sizes and vertical structures of the rings. More recent studies have shown that a larger number of rings are shed each year than previously thought (Goni and Johns, 2001) and that NBC rings exhibit a surprising degree of variability in their vertical structures (Wilson *et al.*, 2002). These findings have reopened the issue of the interhemispheric mass transport by the rings and cast into doubt some of the earlier estimates that had been based on very limited data. Foremost among the limitations of the earlier studies was a lack of *in-situ* sampling in NBC rings, which prevented a detailed assessment of the watermass properties of the rings and the volumes of South Atlantic water they trap and transport northward.

The purpose of this work is to provide a first assessment of the amount of South Atlantic water contained in NBC rings that were observed by both ships and moored time series data as part of the 1998-2000 North Brazil Current Rings (NBCR) Experiment. The NBCR Experiment utilized a variety of observational techniques including shipboard hydrographic and ADCP surveys, moored current meters and IESs, floats and drifters, and remote sensing observations, to study the variability of the retroflexion and the NBC ring generation process. A total of 16 different NBC rings were identified during the experiment, of which four were surveyed in detail by ship. The watermass properties observed in the rings are used herein to make the first quantitative estimates of the trapped core volumes of NBC rings, and are combined with new estimates of the ring formation rate to generate an updated estimate of the annualized South Atlantic water transport by NBC rings.

## 2. DATA AND METHODS

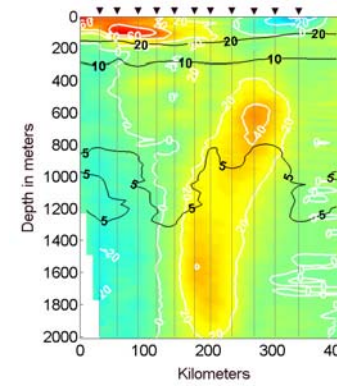
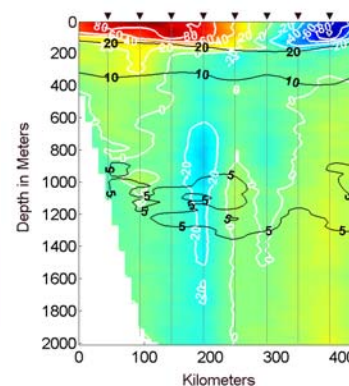
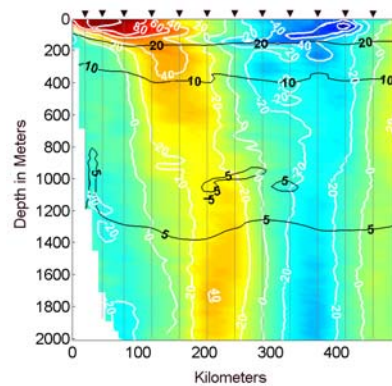
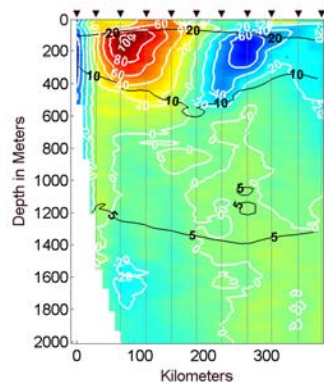
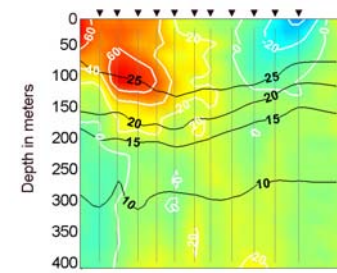
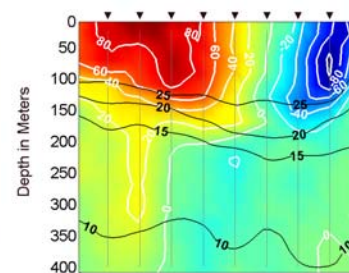
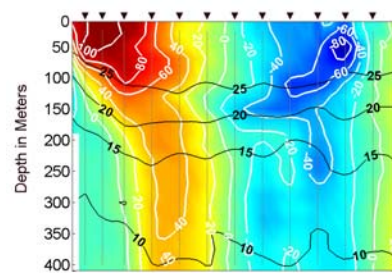
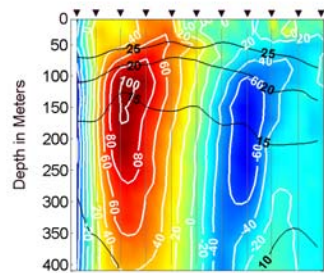
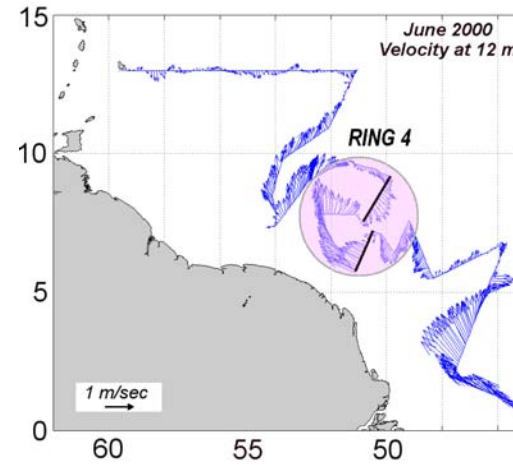
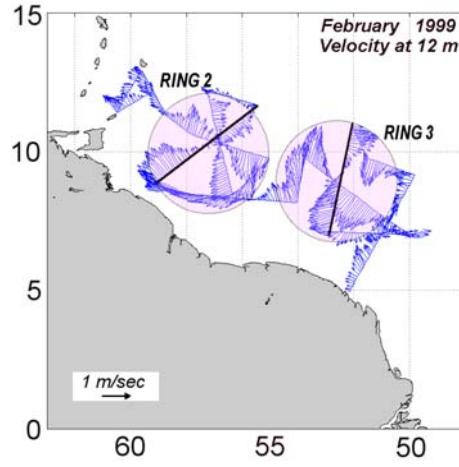
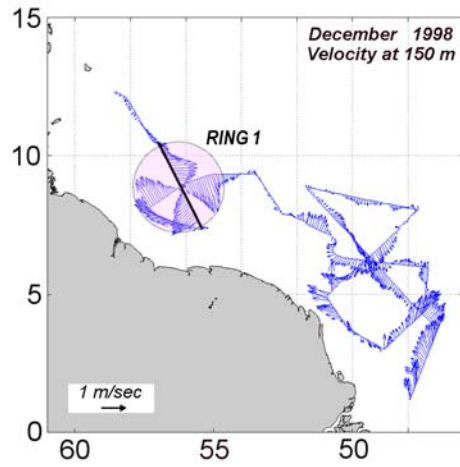
### 2.1 Shipboard surveys

Four cruises were conducted as part of the NBCR Experiment, which took place in (i) November-December 1998, (ii) February-March 1999, (iii) January-February 2000, and (iv) June 2000. Shipboard Acoustic Doppler Current Profiler (ADCP) surveys of the NBC retroflection and translating rings were made on each cruise, using a hull-mounted R.D. Instruments narrow-band 150 kHz ADCP. Conductivity-Temperature-Depth-Dissolved Oxygen (CTDO<sub>2</sub>) stations were occupied at selected locations along the cruise tracks using a dual Seabird 911+ pumped seawater system, and simultaneous lowered-ADCP (LADCP) direct velocity profiles were acquired at all stations from either a 150 or 300 kHz downward-looking ADCP mounted on the CTD package. The CTDO<sub>2</sub>/LADCP profiles were collected to a maximum depth of 2000 m, or to within 10 m of the bottom in water depths less than 2000 m. Water samples were collected from a 24 bottle rosette sampler and analyzed for salinity and dissolved oxygen concentration, which were subsequently used to calibrate the CTDO<sub>2</sub> profiles. Details of the data processing and calibrations are given in Fleurant *et al.* (2000a,b).

During the cruises, four NBC rings were found in the region between 6°-10° N that had clearly detached from the retroflection. Each of these rings was surveyed with multiple shipboard ADCP transects and a closely spaced (20 km) CTDO<sub>2</sub>/LADCP section taken through the center of each ring (Figure 1). Initial results from these ring surveys have been described in Wilson *et al.* (2002). Of the four rings surveyed, two were strongly surface trapped (Rings 3 and 4, in February 1999 and June 2000, respectively; Figure. 1), with their identifiable velocity structure confined above 200 m. Another ring (Ring 1, December 1998) showed an unusual (and previously unobserved) vertical structure; its velocity core was located in the thermocline, at about 150 m, and the magnitude of the ring swirl velocity decreased both upward and downward from that level. The fourth ring (Ring 2, February 1999) presented a strong barotropic structure, with 2000 m velocities larger than 20 cm/s. All of the rings showed a relatively weak thermocline depression of only about 50-75 m at their center, except for the subsurface ring, which had a reversed sense of displacement (a doming of the upper thermocline) due to its subsurface intensified nature, and a larger compensating depression of the deeper isopycnals (~10° C) of nearly 200 m.

### 2.2 Moored time series observations

An array of 16 moored inverted echo sounders (IES) was deployed in the retroflection region to monitor the zonal displacement of the NBC and the formation of NBC rings (Figure 2). Initial results from the IES/PG array are presented in Garzoli *et al.* (2002; this volume) and Garzoli *et al.* (2003). In



addition, two subsurface moorings with current meters and temperature-salinity recorders were deployed directly in the path of translating rings near 9° N, 53° W (Figure 2). The location for these moorings was chosen based on previous analysis of altimetric data and other available results to lie along the center of the mean translation track of NBC rings just after their separation from the retroflection. These time series provided vertical profiles of azimuthal velocity and watermass properties as rings translated past the location of the moorings.

The two moorings were deployed side by side within 3 km of each other (Figure 3). One mooring provided current measurements from 8 conventional current meters (Vector Averaging Current Meters; VACMs) topped by an upward looking 150 kHz ADCP mounted at 250 m; the other mooring provided temperature and salinity time series in the upper ocean between depths of 50 to 1000 m from an array of 10 Seabird Seacat and Microcat recorders. Pressure values were recorded by each of the Seacat/Microcats and a pressure gauge at the top of the current meter mooring to keep track of mooring motion and the measurement depths of the sensors. Maximum vertical excursions of the moorings were 160 m during two short-term events with smaller r.m.s. values of about 30 m. The entire moored array was deployed for a 20-month period from November 1998 to June 2000 (except for the PG that was deployed in February 1999).

The overall data return from the moored array was excellent. Full data records were obtained from all of the IESs and all of the current meters including the upward looking ADCP at the top of the CM mooring. On the adjacent CTD mooring, one sensor failed (at 100 m nominal depth), and two others had short records that ended about mid-way through the deployment. The remaining sensors returned full records and the CTD sensors showed no obvious salinity drift due to biofouling (a testament to the effectiveness of the anti-biofouling tubing used on the conductivity cells). As a result, the current meter and CTD moorings provide a unique record of the velocity and watermass structure of more than a dozen NBC rings that passed over the mooring site. Figure 4 shows the time series of the vector velocity (“stick” plots) from the upper levels of the current meter mooring, in which the signatures of NBC rings are shown by the reversals in flow from an offshore to onshore direction as the rings pass over the mooring location. In Figure 2 the tracks of NBC rings identified from satellite

Figure 1. Top panels: Velocity vectors along the cruise track at 150 m (Ring 1) and at 12 m (Rings 2-4) derived from 150 kHz hull-mounted ADCP on the R/V Seward Johnson during cruises in December 1998 (Ring 1), February 1999 (Rings 2 and 3), and June 2000 (Ring 4). The locations of the rings are shown by shaded circles. Lower Panels: Tangential velocity and temperature along cross-ring sections (Rings 1-4, from left to right) shown by the bold lines in the upper panels. The velocities are based on LADCP data below 30m and shipboard ADCP data from 8-30 m. Velocity contour level is 20 cm/s; temperature contour level is 5°C and inverted triangles on top of each section denote the location of CTD stations (after Wilson *et al.*, 2002).

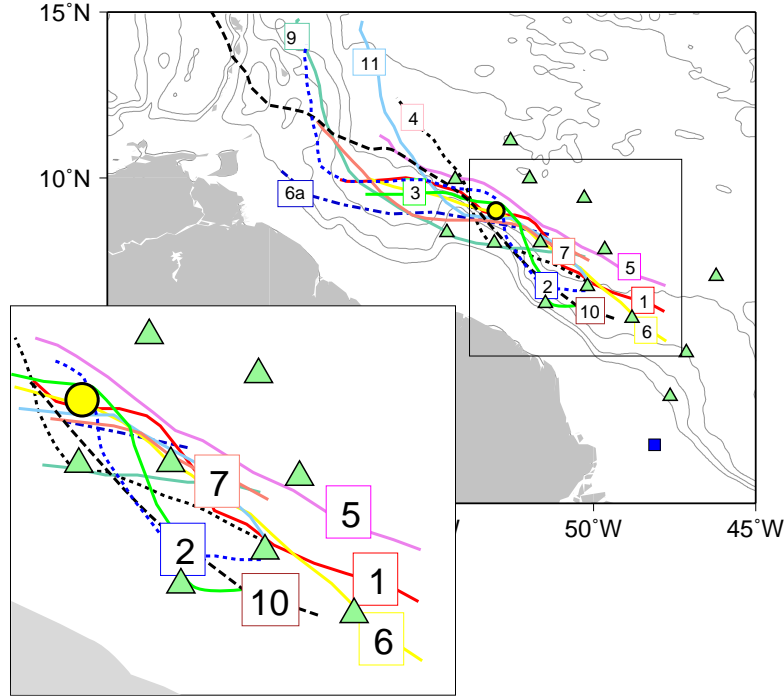


Figure 2. Tracks of NBC rings identified by altimetry during the period of the NBCR Experiment. The numbers on the tracks correspond to the rings listed in Table 2. The symbols indicate the locations of the CM/CTD mooring pair (circle), the array of inverted echo sounders (triangles), and bottom pressure gauge deployed on the Brazilian shelf (square).

altimetry during the experiment are superimposed on the moored array sites, showing that most of the rings passed very close to the CM/CTD mooring site.

### 2.3 Water mass identification

In the remainder of this paper we will use watermass characteristics to distinguish between thermocline waters in the study region that are of South Atlantic and North Atlantic origin. Waters of South Atlantic origin crossing the equator in the NBC carry a distinctive T/S/O<sub>2</sub> signature, being relatively fresher and higher in dissolved oxygen compared to waters from the North Atlantic on the same density surfaces (Wüst, 1964; Emery and Dewar, 1982; Schmitz and Richardson, 1991; Wilson *et al.*, 1994; Bourles *et al.*, 1998). Rings that pinch off from the NBC retroflection are expected to carry waters with this South Atlantic signature into the North Atlantic and therefore have anomalous properties with respect to the surrounding waters.

Traditionally, temperature-salinity (T-S) diagrams are a common tool used for water mass identification. An equivalent approach that contains the same information is to plot salinity versus sigma-theta ( $S-\sigma_\theta$ ), which is more convenient for the purposes of this paper. Figure 5 shows a scatter plot of  $S-\sigma_\theta$  from the more than 200 CTD casts collected in the study region during the four

cruises. All the curves have the same general characteristics: a salinity maximum in the upper thermocline located between  $\sigma_\theta = 24.5$  to  $25.5$  (~100-150 m), corresponding to Subtropical Underwaters (SUW) that are formed in both hemispheres, and an intermediate salinity minimum at  $\sigma_\theta \sim 27.25$  (~800 m) that corresponds to Antarctic Intermediate Waters (AAIW), or Subantarctic Mode Waters, that are formed in the southern hemisphere. Deeper in the water column the salinity increases again to a maximum corresponding to North Atlantic Deep Water (NADW), and then toward the fresher Antarctic Bottom Waters (AABW). Superimposed on the plot are S- $\sigma_\theta$  curves from Levitus (1982) that show the climatological water mass properties at a point on the equator near the western boundary ( $0^\circ$ ,  $40^\circ\text{W}$ ), and at a point in the western North Atlantic north of the NBC retroflexion ( $13^\circ\text{N}$ ,  $50^\circ\text{W}$ ). These curves show that the waters originating from the South Atlantic are fresher on all density surfaces from the AAIW up to near the sea surface ( $\sigma_\theta \sim 24.0$ ). In the surface

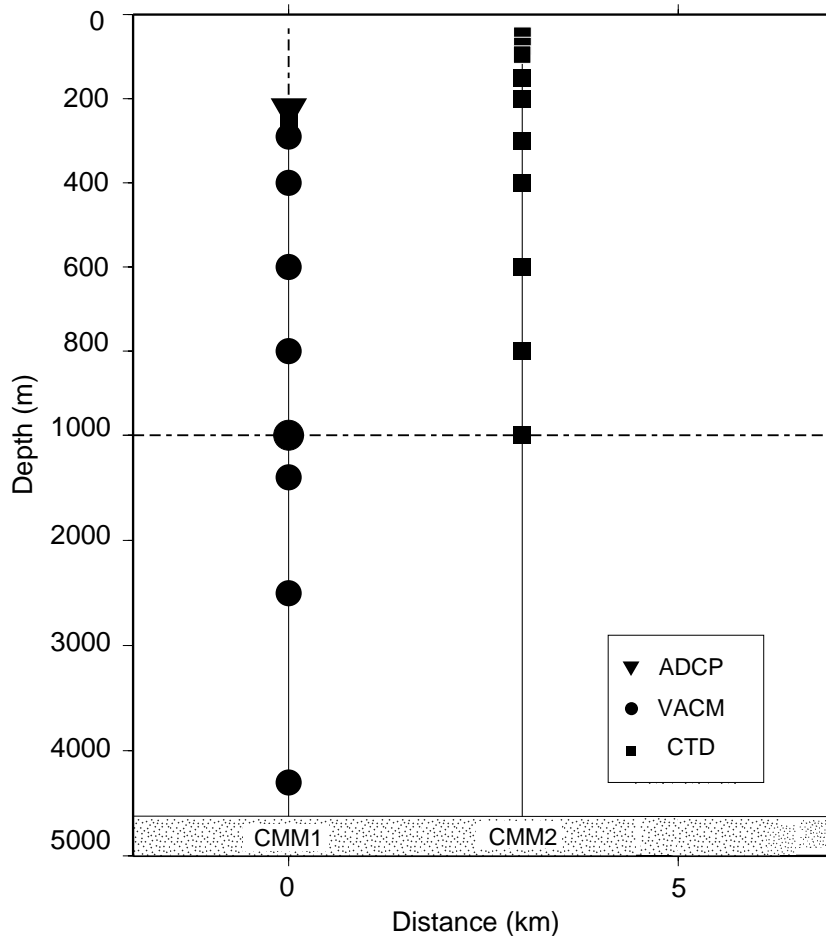


Figure 3. Instrument configuration on the pair of subsurface moorings deployed along the NBC ring translation path. The current meter mooring (CMM1) had conventional current meters at 8 levels through the water column and an upward-looking ADCP profiling to the surface. The CTD mooring (CMM2) had Seabird Microcat and Seacat temperature-salinity-pressure recorders at 10 levels through the upper 1000 m.

layer above  $\sigma_\theta = 24.0$  this distinction breaks down, owing to the freshwater input to the surface layers north of the equator by precipitation under the ITCZ and additional large freshwater inputs from the Amazon River.

To obtain watermass “endpoints” that are representative of South and North Atlantic source waters, we use our own CTD data and construct mean  $S$ - $\sigma_\theta$  curves from the data that are given by the mean of the highest 10% and lowest 10% of the salinity values observed on each density surface. That is, for any given density surface, a “southern” endpoint is constructed by averaging the 10% lowest salinity values observed from all CTD casts, and a “northern” endpoint is constructed from an average of the 10% highest salinities that are observed on that density surface. The CTD casts collected during the program extend from the equator to 13° N and provide a representative sampling of the water

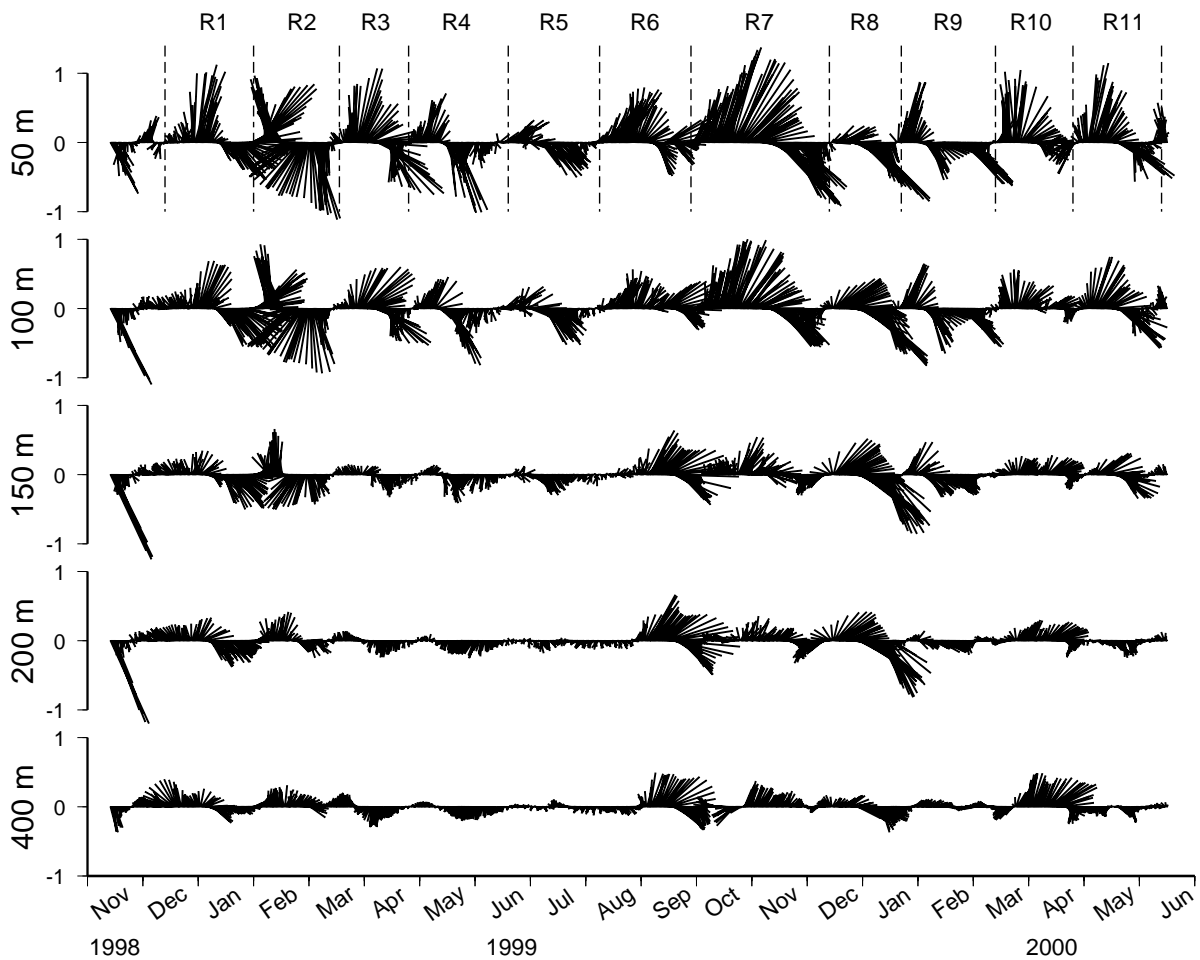


Figure 4. Current vectors from five levels (50 to 400 m) on the CM mooring located in the ring translation corridor. The vectors are rotated 25 degrees from east so that “up” is 025° T, which is normal to the average direction of ring translation. The surface rings that formed during the experiment and passed over the mooring site are labeled chronologically at the top.

masses in the region from different seasons. The resulting “endpoint”  $S-\sigma_\theta$  curves are shown in Figure 5 along with their  $\pm 1$  standard deviation envelopes. The southern endpoint closely follows the southern Levitus curve, while the northern endpoint is saltier than the northern Levitus curve. This probably indicates that the Levitus curve from  $13^\circ\text{N}$  already includes a mixture of northern and southern source waters. These endpoint  $S-\sigma_\theta$  curves are then used to determine the percentage of South Atlantic Water (SAW) contained in any particular CTD cast. Denoting the northern and southern endpoint curves by  $S_N$  and  $S_S$ , respectively, the percentage of SAW on any density surface with a

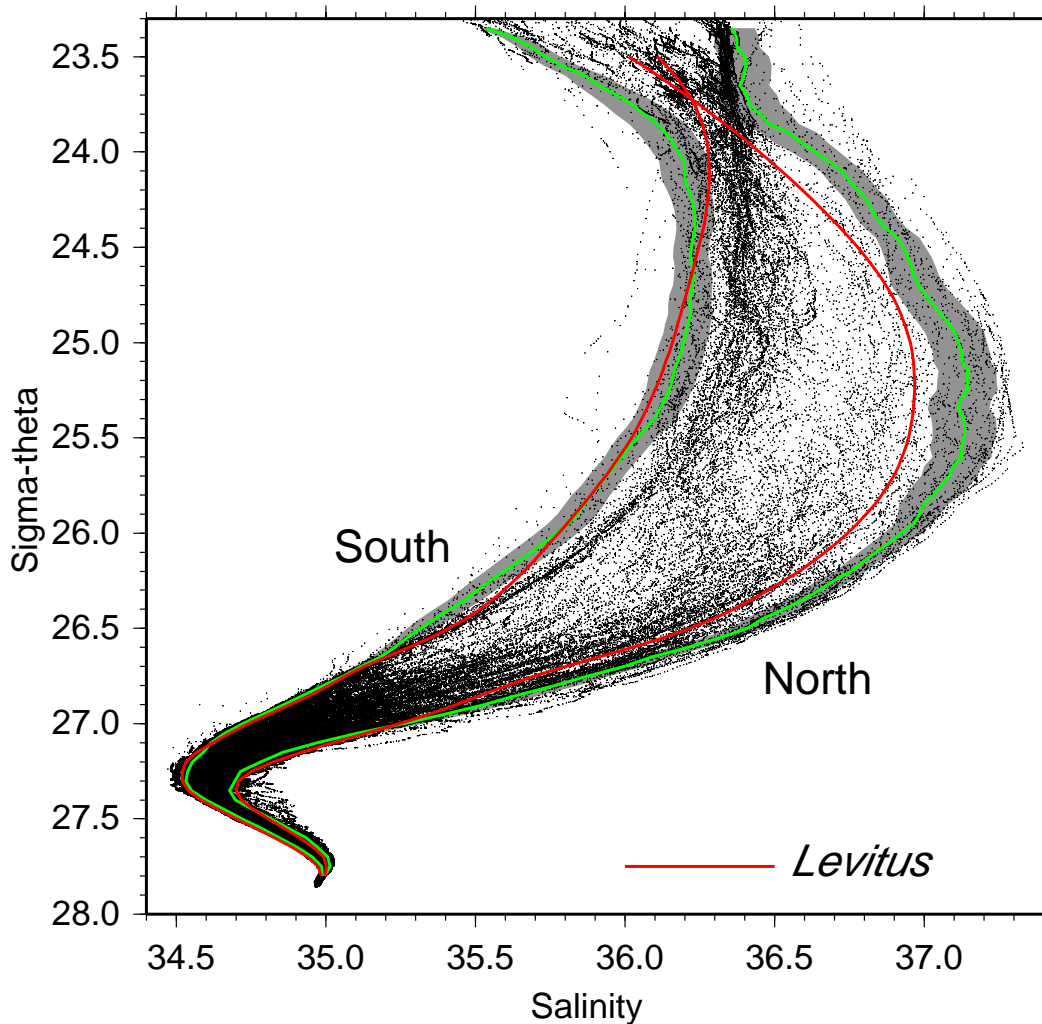


Figure 5. Watermass  $S-\sigma_\theta$  “endpoints” representative of South Atlantic and North Atlantic water properties (green curves) derived from the ensemble of CTD profiles collected during the NBC Rings Experiment (shown by scatter). The shaded envelopes show the one-standard deviation envelopes of the endpoint watermass curves. The red lines are taken from the Levitus climatology at  $0^\circ$ ,  $40^\circ\text{W}$  (“South”) and  $13^\circ\text{N}$ ,  $50^\circ\text{W}$  (“North”).

salinity value  $S$  is simply proportional to the inverse linear distance from the endpoint curves:

$$\text{SAW}\% = (S_N - S) / (S_N - S_S) \cdot 100 \quad (1)$$

This procedure is assumed to be valid for all density surfaces between the AAIW level ( $\sigma_\theta = 27.2$ ) and the top of the main thermocline ( $\sigma_\theta = 24.5$ ), but is not applied above  $\sigma_\theta = 24.5$  due to the ambiguity in defining the water mass source above that level. If the observed salinity value is higher or lower than the endpoint curves within the  $\sigma_\theta = 24.5$  to  $27.2$  range, we assign it to be “pure” (i.e., 100%) northern or southern source water, respectively. In general, any particular CTD cast in the region will have a variable percentage of SAW through the water column as the two water masses interleave and mix.

A similar approach can be developed using dissolved oxygen data, where the South Atlantic waters exhibit high dissolved oxygen content compared to North Atlantic waters. Qualitatively this yields similar results, however, since the dissolved oxygen concentration is non-conservative this approach is less quantitative. Also, we wish to apply this same approach to the moored CTD time series observations, where only T-S data is available, therefore for consistency we use the above approach based on the  $S$ - $\sigma_\theta$  relationship.

### 3. RESULTS

#### 3.1 Surveyed rings

During the four research cruises conducted as part of the NBC Rings Experiment, four NBC rings were found and surveyed (Table 1). During the first cruise (November 7 – December 11, 1998) one ring was found (Ring 1); during the second cruise (February 6 - March 9, 1999) two rings were found (Rings 2 and 3), and during the fourth cruise (June 7-23, 2000) one additional ring was found (Ring 4). A fifth ring was observed to nearly pinch off from the retroflection on the third cruise (January 29 - February 24, 2000), but it failed to pinch off in time to be considered a fully separated ring.

Examples of the CTDO2/LADCP sections taken across two of the rings (Rings 1 and 2) are shown in Figure 6, which is used to determine the deep flow structure and watermass characteristics in the rings. For Ring 1, 11 stations were taken in a SE-NW direction across the diameter of the ring, extending from both edges of the ring where the swirl velocities decreased below about 15 cm/s. This ring was the only subsurface ring to be surveyed by ship, and due to its unusual vertical structure it was only confirmed as an NBC ring after its watermass signatures were examined. The  $S$ - $\sigma_\theta$  curves for these stations (Figure 6, bottom right panel) show water properties predominantly of North Atlantic origin near the periphery of the ring and South Atlantic origin near the ring core. Stations 62-64 near the ring core all have a very strong SAW signature

from  $\sigma_\theta = 24.5$  to  $27.0$  (approximately 50-500 m). Stations farther out from the center but inside the radius of maximum velocity of the ring (indicated by the inner circle drawn in Figure 6, top left panel) also show strong SAW characteristics but over a smaller depth or density range than the core stations.

Ring 2 (Figure. 6, right panel), which was a more typical surface-intensified ring but with a deep-reaching velocity structure, was sampled by 14 stations across the diameter of the ring. The stations near the center of this ring also show strong SAW characteristics, but in contrast to Ring 1 these strong characteristics are more confined to the surface layers, above  $\sigma_\theta \sim 26.0$ . Deeper in the water column, below  $\sigma_\theta = 26.5$ , SAW characteristics again become evident at the core stations with considerable interleaving of North Atlantic waters.

To quantify the amount of SAW contained in the rings, the percentage of SAW at each station as determined by the procedure outlined above was integrated over the total volume of each ring. The limits of the integration are

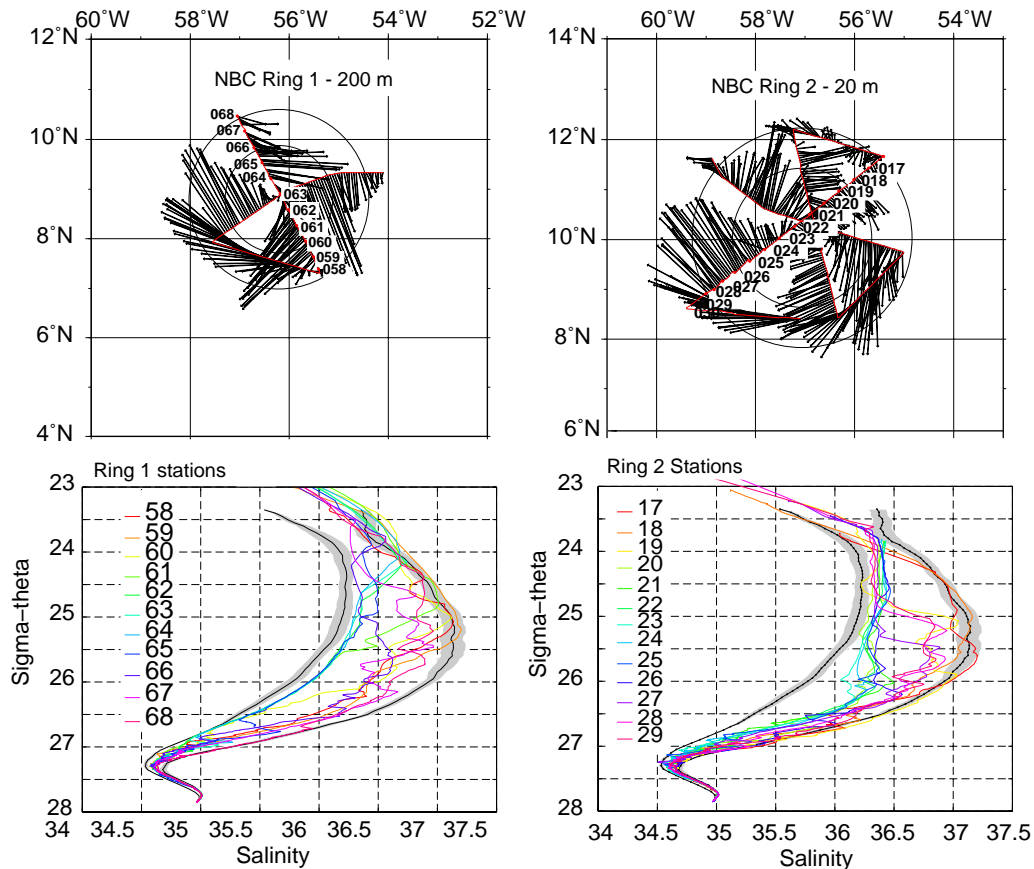


Figure 6. Near-surface (20 m) current vectors from shipboard ADCP for Rings 1 (left panels) and 2 (right panels), showing locations of CTD/LADCP stations across the ring (top), and  $S-\sigma_\theta$  profiles for the ring CTD stations (bottom), superimposed on the South Atlantic and North Atlantic watermass curves from Figure. 5.

set by the physical characteristics of the ring, which were defined as follows. The **edge radius** of the ring is defined as the location where the swirl velocity at the core depth of the ring drops below a value of 15 cm/s, averaged around the perimeter of the ring. (The core depth of the ring is the depth where the swirl velocity of the ring is a maximum – usually at the surface except for subsurface rings.) The **radius of maximum velocity** (hereafter  $r_{\max}$ ) is the average distance from center of the ring to the maximum swirl velocity, again averaged around the ring at the core depth. The **vertical penetration**, or depth limit, of the ring is defined as the depth below which the swirl velocity drops to less than 10 cm/s. An upper limit may also exist for subsurface rings. The choices of the velocity cutoffs for the outer edge (15 cm/s) and vertical penetration (10 cm/s) of the rings are made to ensure that only waters that are circulating with the ring are included in the ring volume calculations.

Integration of the SAW volume of each ring is then carried out over limits set by the vertical scale and the edge radius of the ring. For depths in the rings shallower than the  $\sigma_\theta=24.5$  surface (~50-100 m), the percentage of SAW determined at the  $\sigma_\theta=24.5$  surface for each station is assumed to remain constant to the surface. Since the South and North Atlantic waters are indistinguishable above this level from their T-S properties, we are thus assuming that the near surface waters circulating in the cores of surface-intensified rings have SAW percentages at least as high as those in the layers immediately below. For rings that penetrate deeper than 1000 m (of which we observed only one), the integration is stopped at 1000 m, since we are concerned only with the transport of upper ocean waters (at the AAIW level and above) by the rings. Usually only one full section was taken through each ring, and therefore an assumption about the geometry of the rings is needed. In the following calculations we assumed a semicircular symmetry for the rings, such that the section taken across a diameter of each ring samples two “halves” of the ring. Each station at a particular radial distance from the center of the ring is therefore assumed to be representative of the water properties on that side of the ring. Most of the rings observed appeared to be nearly circular in shape, which supports this assumption. However, not all of the rings show a symmetric distribution of SAW percentage across the ring, and the above method allows a better estimate of the volume of SAW in a ring to be obtained than could be made from a single radial section.

Examples of the SAW distribution across Rings 1 and 2 and the associated ring velocity structures are shown in Figure 7. In Ring 1 the ring swirl velocity is a maximum at 150 m and it extends to almost 600 m before dropping to insignificant values. Waters with SAW percentage in excess of 90% are found throughout the core of the ring from depths of 150 m to greater than 500 m. Near the surface the SAW percentage is smaller which is consistent with the subsurface intensified structure of the ring. A close correspondence can be seen between the horizontal limits of the SAW distribution and the location of the swirl velocity maximum ( $r_{\max}$ ), which is typical of most of the rings observed.

Significant amounts of SAW are also found below the ring, but since these waters are not clearly rotating with the ring they are excluded from the SAW volume calculation.

Ring 2 has a very different distribution of SAW but one that also closely follows the velocity distribution of the ring. In the surface layers the SAW percentage is relatively high, between 60-90% (which is mostly extrapolated upward from the  $\sigma_\theta = 24.5$  level), and the edges of the SAW distribution coincide with the swirl velocity maxima. Deeper in the water column the ring has a smaller diameter than at the surface and the SAW distribution similarly contracts to occupy mostly the core region between the deep swirl velocity maxima. Relatively high amounts of SAW are found in the ring core to depths including the AAIW layer. Just below the surface layer, at about 200 m, there is a thin layer of lower SAW percentage across the whole ring that appears to separate the upper and lower cores. This layer occurs at the base of the strongest vertical shear in the upper part of the ring and suggests that enhanced mixing of North Atlantic waters into the core of the ring may be occurring there.

Rings 3 and 4 (not shown) were surface-intensified rings like Ring 2 but penetrated less deeply than Ring 2, to depths of approximately 400 m and 200 m, respectively (Table 1). The parameters for all four of the ship-surveyed rings are listed in Table 1, along with the volume of SAW they contain according to the integration procedure described above. The volume of SAW contained in each ring can also be expressed in terms of an equivalent “annualized” volume transport associated with each ring (the last column of Table 1), which is simply the volume of SAW in the ring divided by the number of seconds in one year.

Of the four rings, Ring 2 had the largest volume of SAW ( $4.6 \times 10^{13} \text{ m}^3$ , or an annualized transport of 1.5 Sv) and Ring 4 had the smallest volume ( $2.1 \times 10^{13} \text{ m}^3$ , or 0.7 Sv; Table 1). Ring 3 contained nearly as much SAW volume as Ring 2, even though it penetrated much less deeply and had a slightly smaller  $r_{\text{max}}$  (150 km vs. 160 km). This was due to a larger amount of SAW in the outer parts of Ring 3 beyond  $r_{\text{max}}$ , which could be related to the fact that Ring 3 was “younger” when surveyed and may have had less mixing of North Atlantic waters occur on its periphery than for Ring 2. This points up one of the issues with quantification of the SAW volumes carried in these rings; that the surveys can be completed at different stages in the rings’ lifetimes. Rings that are older may have already lost considerable amounts of SAW to mixing compared to the time they were formed. Ring 1 also contained a SAW volume similar to that of Ring 2 (and Ring 3), owing to the thick layer of nearly pure SAW in its core, even though its  $r_{\text{max}}$  was substantially smaller (100 km) than that of the other rings.

### 3.2 Rings identified by moorings

From the moored CM/CTD data we were able to identify 14 anticyclonic features that passed over the mooring site during the period of the observations (Figure 8; see also Figure 4). Based on comparisons with the IES and altimetric

observations and the *in-situ* water mass properties we interpret all of these features to be NBC rings. (Note that the rings observed by the moorings are labeled chronologically, *and independently*, of the ship-surveyed rings, and are denoted by the prefix “R” hereafter to avoid confusion.) Of the 14 rings observed by the moorings, 11 had a strong surface signature and could also be identified in the IES and/or altimetry data (Garzoli *et al.*, 2002; Goni and Johns, 2002), while 3 were subsurface rings (labeled with an “a” in Figure 8) that had no clear surface signature. These features appear to be variants of the single subsurface-intensified ring we found and surveyed on the first project cruise (Ring 1 above), which had pinched off before the moored array was first deployed. (The signature of that ring can be seen at the very beginning of the CM record, where only the onshore flow associated with the trailing edge of the ring was observed.). A similar approach to that used in the surveyed rings is applied here to the moored CM/CTD data to estimate the SAW volumes carried in these rings. We use the IES data to determine the average translation speeds of the rings as they pass by the mooring location, which allows the mooring data to be cast in terms of virtual “sections” through each ring. Although this method is more approximate than the estimates derived for the ship-surveyed rings, it greatly increases the sample ring population and helps us to arrive at better statistics and more reliable estimates of the average SAW transport carried by the rings. The steps in the procedure are as follows:

1. Synoptic maps of thermocline depth derived from the IES array (Garzoli *et al.*, 2002) are used to determine the average translation speed of each ring during the time period it passes over the mooring (Table 2). The time series data from the CM and
2. CTD moorings are then mapped into a spatial coordinate relative to the “center” of each feature (which is defined by the reversal in cross-shore velocity component).
3. The SAW percentage at each moored CTD sensor is determined in the same manner as for the shipboard CTD profiles, although this calculation can now only be performed at the discrete depths where the sensors were located. A vertical profile of SAW percentage is then created by linear interpolation (in density coordinate) of the SAW percentage observed at the various sensors. This profile is then mapped into a depth coordinate using the known depths of the sensors.
4. The SAW volume is integrated over the volume of each feature, using the same definitions and procedures defined for the ship-surveyed rings.

For the subsurface rings we do not have an independent estimate of their translation speeds, and so we assign a translation speed to them equal to the average translation speed of the surface rings (12.5 km/d). This is really only a guess but it yields  $r_{\max}$  values for these features in the range of 90-105 km, consistent with the observed  $r_{\max}$  of the one subsurface ring surveyed by ship

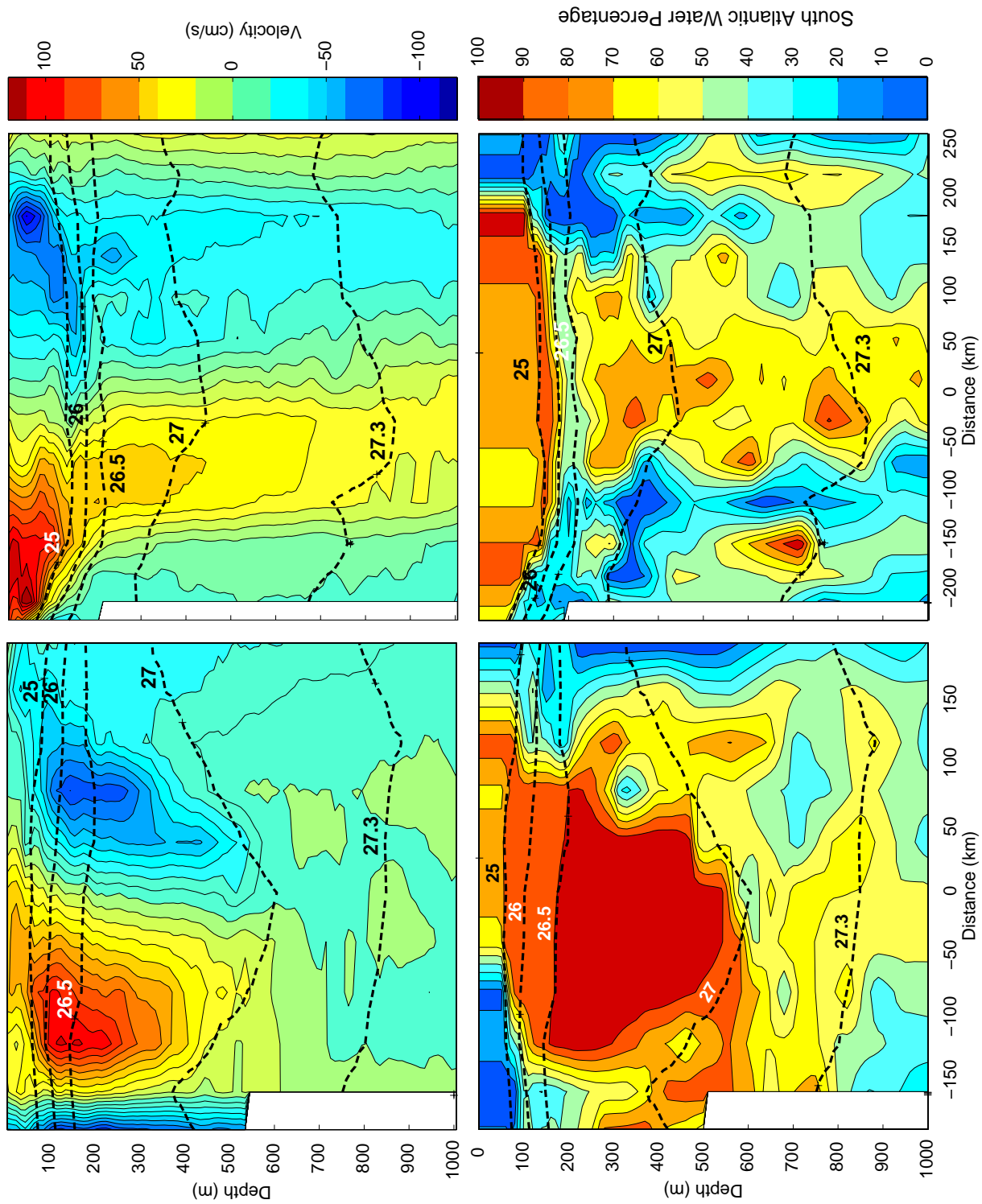


Figure 7. Cross-sections of tangential velocity (top) and South Atlantic Water percentage (bottom) of ship-surveyed Ring 1 (left) and Ring 2 (right). The dashed lines show  $\sigma_0$  surfaces across the ring. The dashed lines show  $\sigma_0$  surfaces across the ring.

Table 1.

Ring parameters for the NBC rings surveyed during the cruises. The last two columns refer to the volume and associated transport of South Atlantic waters in each ring.

Ring	Date surveyed	Vertical penetration (m)	Radius of max velocity (km)	Volume ( $10^{13}\text{m}^3$ )	Annualized transport (Sv)
1	09-Dec-98	50-580	100	4.1	1.3
2	12-Feb-99	0-2000	160	4.6	1.5
3	18-Feb-99	0-350	150	4.4	1.4
4	12-Jun-00	0-200	150	2.1	0.7

(100 km). The one additional difficulty associated with this method is the uncertainty in the track of each ring and how closely the ring centers pass to the mooring site. Some information can be gained from the altimetry and IES data on how close the center of the rings pass to the mooring site, but the absolute accuracy of the ring center location and its track derived from either method is probably not better than 50 km. The tracks derived from altimetry (see Figure. 2) as well as IES nevertheless suggest that all but three of the rings passed within 50 km of the CM/CTD mooring site.

The proximity of the rings to the mooring site can also be inferred from the moored current meter data itself by the sense of rotation of the current vectors as the rings pass by it. A rotation of the current vectors in a clockwise direction indicates a passage of the ring center shoreward of the mooring location; likewise a counterclockwise rotation of the vectors indicates a passage of the ring center to the seaward side of the mooring site (Figure 9). The distance by which the ring center misses the mooring site can also be inferred to some extent from the current vectors. For example, a circularly symmetric ring passing to the shoreward side of the mooring site at a distance equal to the  $r_{\text{max}}$  of the ring will produce current vectors that increase to a maximum strength in the SE direction (i.e., in the direction of the swirl velocity on the “right” side of the ring) as the ring center passes, and during the entire passage of the ring the vectors will always exhibit this SE component superimposed on the reversing onshore/offshore flow (see Figure 9). The opposite occurs for a passage of the ring center a distance of  $r_{\text{max}}$  to the seaward side of the mooring location.

In Figure 4 it can be observed that most of the ring passage events show a clockwise rotation of the current vectors, indicating that most of the rings passed slightly shoreward of the mooring location. An exception is moored ring 2 (R2 in Figure. 4), which displays an anticlockwise rotation as the ring passes. Certain

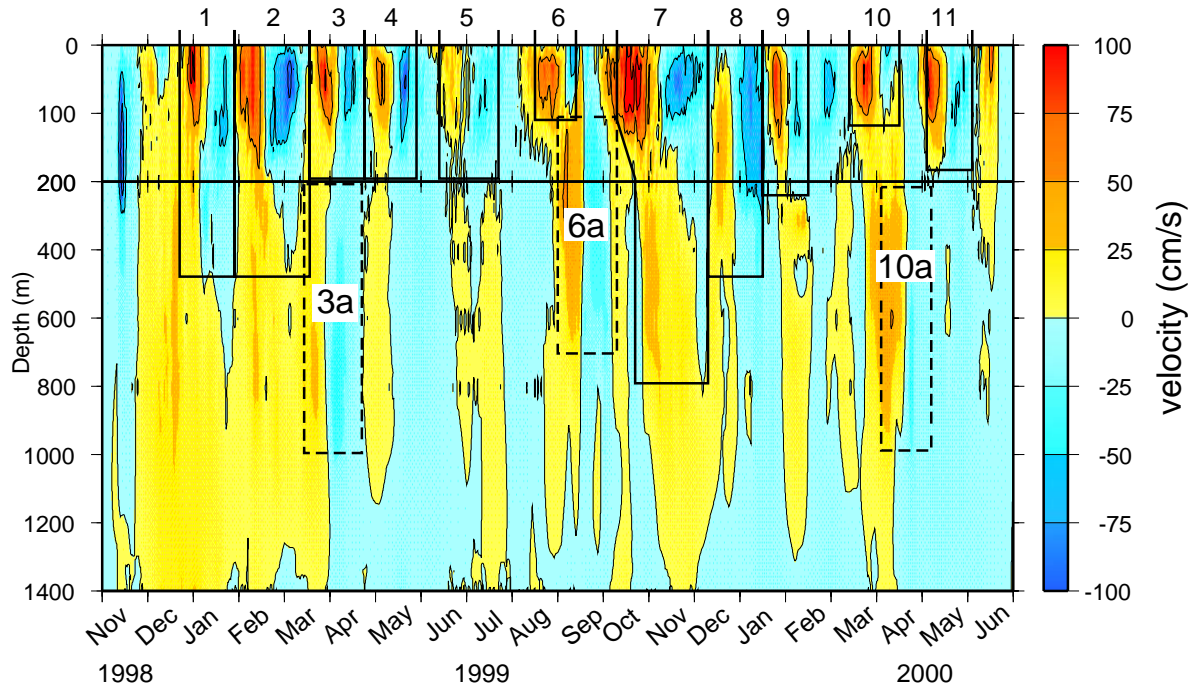


Figure 8. Offshore velocity ( $25^\circ$  T) component at the CM mooring, contoured as a function of depth to 1400 m. The 14 rings identified from the record are labeled by consecutive numbers (1–11) for the surface rings, and 3a, 6a, and 10a for the subsurface rings. The approximate depth limits of the rings are indicated by the boxes drawn around each feature. Note the depth scale change at 200 m.

of the rings (e.g., R5, R8) appear to have passed considerably inshore of the mooring site, at a distance of order  $r_{\max}$  according to their velocity signatures. However, most of the rings passed very close to the mooring site according to their velocity signatures, and all but R5 and R8 passed well within a distance of  $r_{\max}$  from their centers.

Examples of the velocity structure and SAW percentage in three of the rings observed by the mooring are shown in Figure 10. Moored ring 1 (R1), shown in Figure 10 (left panel), is the same ring that was surveyed by ship on 12 February 1999 (ship Ring 2, see Figure 7, right panel). The ring center passed over the mooring site on 11 January 1999, which was about a month before it was surveyed by the ship. A direct comparison of the two figures shows that there are some significant differences between the two realizations. While the velocity distribution in the upper 150 m is similar in both pictures, the signature of the ring in the moored data lacks the deeply penetrating velocity structure found in the shipboard survey. Another difference is that the shoreward flow on the trailing side of the ring at depths of 200–500 m is shifted forward in the ring so that it nearly underlies the surface center of the ring. This suggests that near

Table 2.

Ring parameters for the NBC rings observed by the current meter and CTD moorings. The last two columns refer to the volume and transport of South Atlantic waters in each ring.

Ring	Date	Vertical penetration (m)	Radius of max velocity (km)	Volume ( $10^{13}\text{m}^3$ )	Annualized Transport (Sv)
1	11-Jan-99	0-500	150	3.9	1.2
2	21-Feb-99	0-600	160	5.4	1.7
3	08-Apr-99	0-200	100	1.3	0.4
3a	31-Mar-99	200-1000	90	5.7	1.8
4	14-May-99	0-200	95	0.7	0.2
5	05-Jul-99	0-180	120	0.6	0.2
6	05-Sep-99	0-120	150	1.6	0.5
6a	19-Sep-99	120-800	105	5.3	1.7
7	07-Nov-99	0-800	145	7.2	2.3
8	30-Dec-99	50-500	150	5.0	1.6
9	02-Feb-00	0-250	85	0.9	0.3
10	01-Apr-00	0-130	100	0.8	0.3
10a	14-Apr-00	250-1000	105	6.6	2.1
11	18-May-00	0-180	140	1.9	0.6

the time of its formation the vertical axis of the ring may have been tilted forward with depth in the direction of motion of the ring.

According to our criteria for the penetration depth of the rings, the penetration depth of R1 is only 500 m, compared to 2000 m (or more) for the ship-surveyed ring. The only reasonable explanation we can give for this difference is that the ring must have evolved to a more barotropic structure after it pinched off from the retroflection; that is, a deep component of anticyclonic circulation was somehow spun up under the ring. The SAW distribution is also different in the two realizations, showing a large mass of high SAW percentage on the forward side of R1 at subsurface levels that is mostly outside of the circulation of the ring. Other features of the SAW distribution are similar, including the high SAW percentages in the upper core, the suggestion of interleaving of North Atlantic waters just below this level, and the waters with high SAW percentage found at depth under the ring core. It is interesting that there is a significant amount of SAW in the deeper layers below the main circulation of the ring at the time it was formed, but it is not clear why this occurs. It appears likely that this water was entrained into the deep circulation of the ring as it spun up and was carried northward with the ring.

The SAW volume estimate we derive for R1 is  $3.9 \times 10^{13} \text{ m}^3$  (or 1.2 Sv; Table 2), which is, surprisingly, only about 15% smaller than the estimate derived from

the shipboard survey. This agreement results from the relatively higher percentages of SAW in the subsurface layers on the northern side of R1, that compensate partly for the smaller vertical penetration of R1. This level of agreement may be fortuitous given the differences in the two observed structures and it illustrates some of the uncertainty that is involved in estimating the trapped core volumes of the rings.

The other ring sampled by both moorings and ship was moored ring 2 (R2), which is ship-surveyed Ring 3. In contrast to the above case, this ring was sampled at very nearly the same time by both methods (the ship survey occurred within 3 days of when the ring center passed the mooring site), and the results of the two realizations are in much closer agreement. The structure and SAW distribution of R2 are shown in Figure 10 (center panels). The strong circulation in the ring is mostly trapped to the upper 200 m, with an overall vertical penetration to 600 m according to our velocity criteria. The watermass distribution shows a high percentage of SAW in the ring core extending from the surface layers to depths of about 800 m. Again there are significant amounts of SAW in the core of the ring below our strict cutoff definition of the penetration depth of the ring, which may in fact be weakly circulating as part of the ring. It is possible that our criterion for “significant” mean swirl velocity at the base of the ring (10 cm/s) is too restrictive and may be excluding some of the

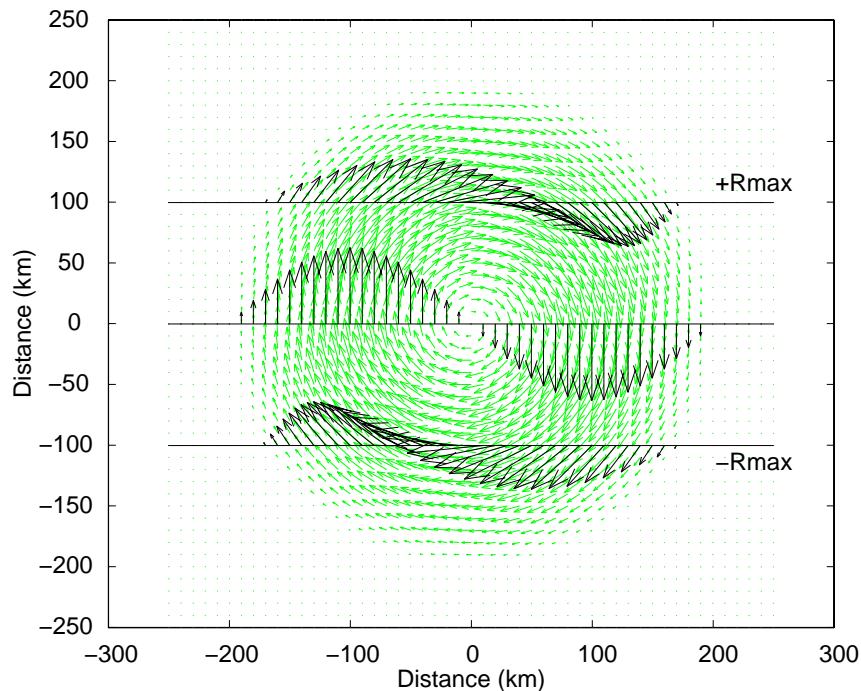


Figure 9. Schematic illustration of a circularly symmetric, anticyclonic ring with a radius of maximum velocity ( $R_{max}$ ) of 100 km. The dark arrows indicate the patterns of current variation that would be observed at a fixed measurement site if the ring passed directly over the site (central line), or if it passed shoreward (top line;  $+R_{max}$ ) or seaward (bottom line;  $-R_{max}$ ) of the site a distance of  $R_{max}$  from the ring center.

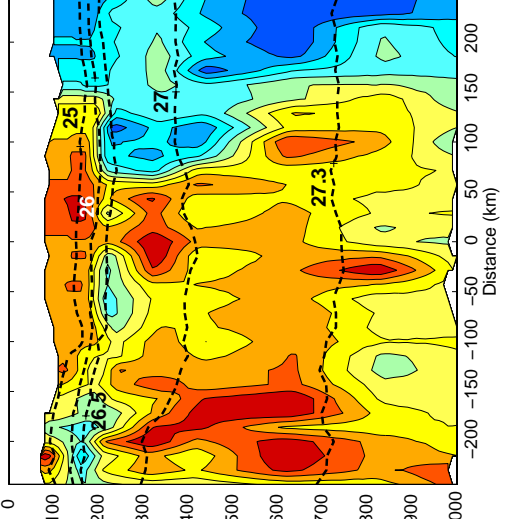
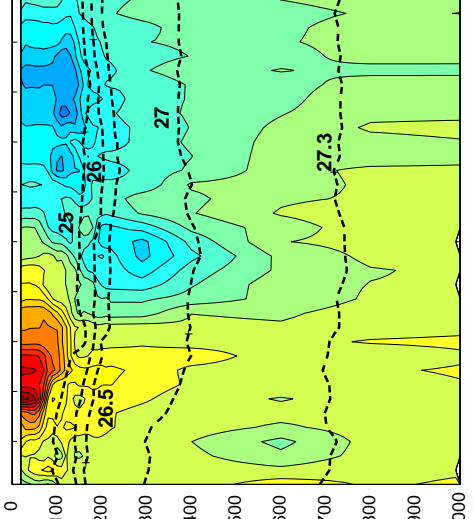
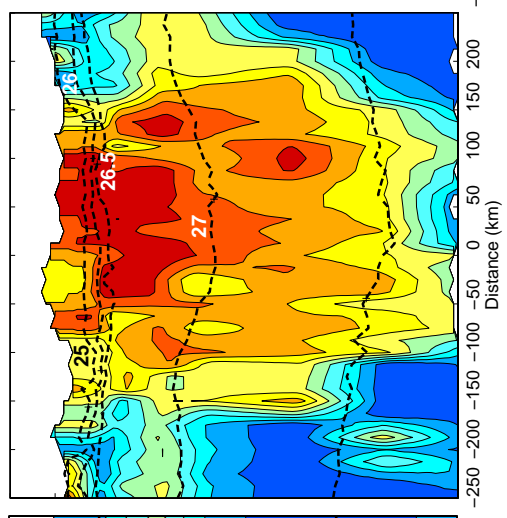
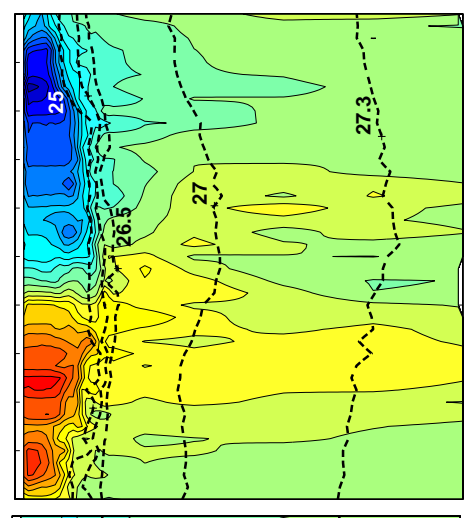
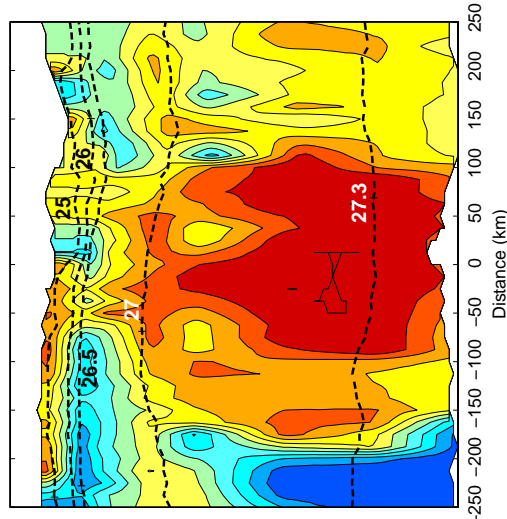
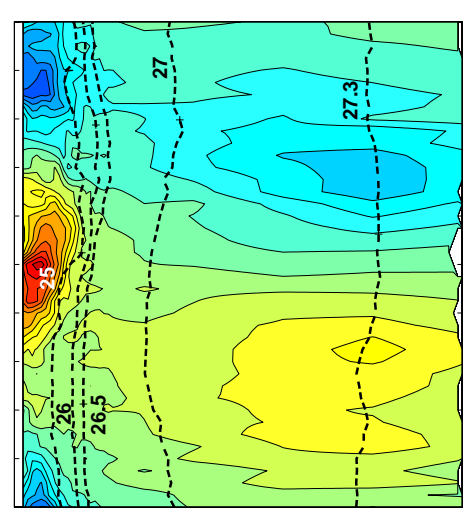
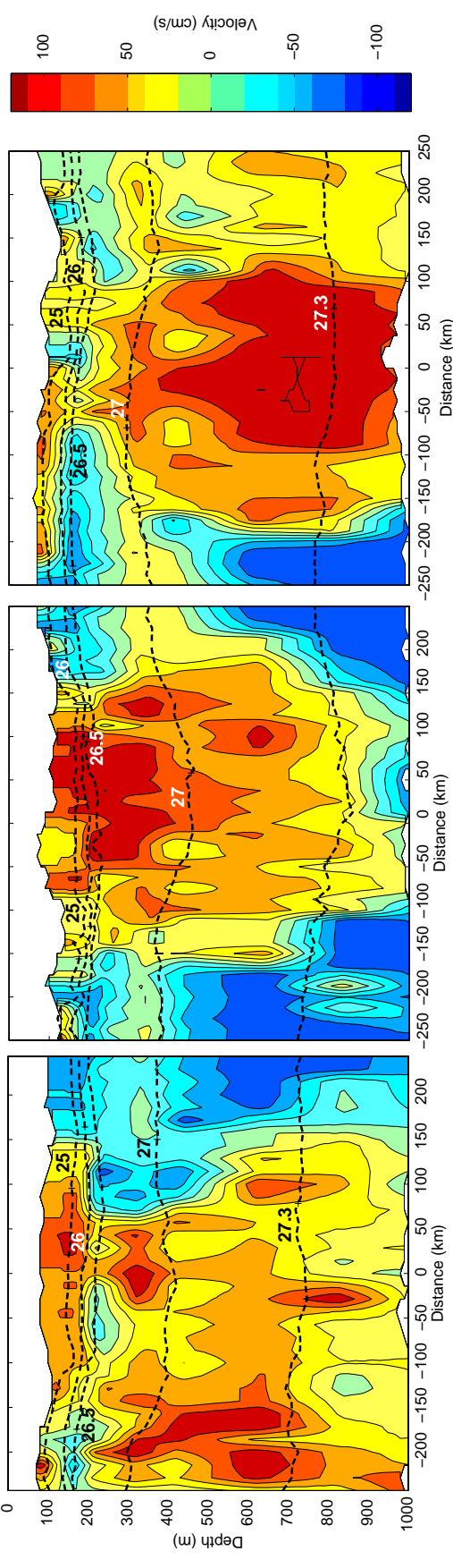
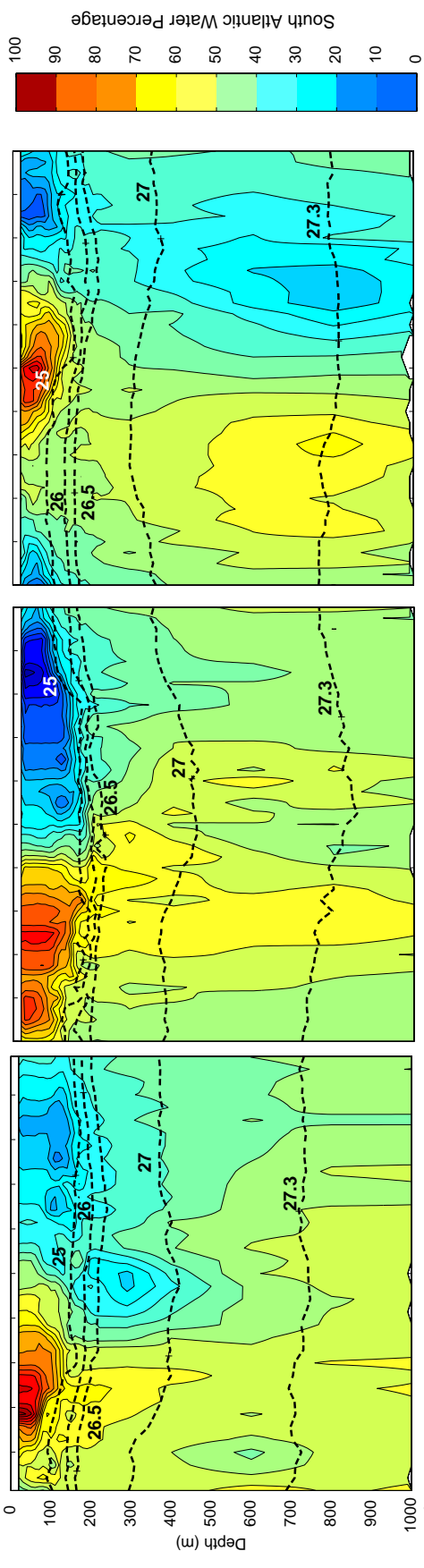
SAW that is transported in some rings. However, we prefer to be conservative in this choice so that only waters that are clearly circulating in the ring are included in the volume integration.

The shipboard survey of this ring (not shown) is very similar to that shown in Figure 10 (center panels) except that the deeper tails of the velocity structure are somewhat weaker, which results in an official penetration depth of 350 m for this ring based on our criteria. This illustrates again some of the difficulty in defining an unambiguous penetration depth of the rings based on their velocity structures. Accordingly, the calculated SAW volume of R2 derived from the moored data is higher than that estimated from the shipboard survey ( $5.4 \times 10^{13} \text{ m}^3$  versus  $4.4 \times 10^{13} \text{ m}^3$ ; Tables 1 and 2).

Finally, we show in Figure 10 (right panels) the structure and SAW distribution of one of the subsurface rings observed by the moorings (R3a; Figure 8). This feature occurred in close proximity to a surface-intensified ring (R3), and it is not completely clear whether these are separate features or if they are physically coupled. However, there is a clear minimum in velocity at about 200 m depth and a lateral offset of about 100 km between the surface and deep velocity cores, which leads us to believe they are distinct features. The other subsurface features that occurred in the record (R6a and R10a) also seemed to be paired with nearby shallow, surface-intensified rings but again appear to be distinct features. The SAW distribution for ring R3a shows a definite core of SAW that is enclosed within the subsurface swirl velocity maxima centered at about 800 m and that fills the water column between 200-1000 m. In the overlying ring (R3) the SAW distribution is actually less well defined than in the subsurface ring and it appears to be separated from the subsurface ring by an intruding layer of North Atlantic water. The volume of SAW in the subsurface ring (R3a) is calculated to be  $5.7 \times 10^{13} \text{ m}^3$  (or 1.7 Sv; Table 2) whereas the surface ring (R3) has a much smaller SAW volume of  $1.3 \times 10^{13} \text{ m}^3$  (or 0.4 Sv). The weaker and more disorganized SAW signature of the surface ring R3 is characteristic of the other shallow and relatively small diameter rings that occur later in the record (i.e., rings R4, R5, R9, and R10), which, interestingly, are all formed in the February to July time frame.

The ring parameters and SAW volume estimates for all of the rings observed by the moorings are summarized in Table 2. The values of  $r_{\text{max}}$  estimated for the surface rings vary from 85 to 160 km, while those for the three subsurface rings are from 90 to 105 km. The observed  $r_{\text{max}}$  values of the surface rings suggests a bimodal size distribution of the surface rings with a tendency

Figure 10 (next page). Cross-sections of tangential velocity (top) and South Atlantic Water percentage (bottom) of rings R1 (left panels), R2 (center panels) and R3a (right panels) observed by moorings. The dashed lines show  $\sigma_\theta$  surfaces across the ring. The SAW percentage in the lower figure is shown only below the level of the uppermost CTD instrument on the mooring, and it is assumed to be constant from that level to the surface. The dashed lines show  $\sigma_\theta$  surfaces across the ring.



for formation of either “large” rings (with typical  $r_{\max}$  of 150 km) or “small” rings (with a typical  $r_{\max}$  of 100 km). As noted above, this distribution also tends to be seasonal, with the large (and more deeply penetrating) rings forming during the fall and early winter months.

It is difficult to place precise error bounds on our SAW volume estimates for the rings, as a variety of uncertainties come into play, including the definitions of the “endpoint” watermass curves, the ambiguity in defining the cutoff depths for the SAW volume calculation, possible ring asymmetries, the manner in which the moorings slice the rings, and the differences found between rings that were sampled by both methods. We estimate an overall uncertainty of  $\pm 30\%$  for the SAW volume of the individual rings surveyed by ship, and up to  $\pm 50\%$  for rings sampled by the moorings. The large population of rings observed by the two methods however helps to compensate for errors in estimating the SAW volume carried by the individual rings.

### 3.3 Cross-gyre transport by NBC rings

A summary of the rings observed by the moorings is given in Table 3, and a summary of all rings observed by ship and moorings during the experiment is given in Table 4. If we consider first the moored observations only and sum the individual ring SAW transports for the 14 rings observed, the total SAW transport over the 20 months of the moored record is 14.9 Sv. This gives an average SAW transport per ring of 1.1 Sv (including all ring types), and an annual SAW transport of SAW by the rings of 8.9 Sv/yr. Incorporating the ship-surveys, which add two additional rings not sampled by the moorings (for a total of 16 rings over a period of 22 months - see Table 4) the respective estimate is 9.3 Sv for the annual SAW transport by rings. These estimates assume that the ring population we observed is representative of the frequency of occurrence of different ring types and that the seasonal bias resulting from incomplete sampling of two full annual cycles is small. The latter estimate derived from the combined shipboard and moored observations is probably better in this regard. The above estimates also assume that the number of rings shed, and the occurrence of different ring types during this  $\sim 2$  year period, is representative of the climatological behavior of NBC ring shedding, which may not be true (see further discussion below).

The rate of NBC ring formation suggested by these observations is about 8.5 rings per year, or one ring every 1.4 months, including all ring types. For the surface-intensified rings, which are most common, this rate is about 6.5 rings per year, or one ring every 1.8 months. For the subsurface rings it is 2 per year. If we subdivide the total SAW transports into the portions corresponding to surface rings and subsurface rings, the annual SAW transport by the surface rings is 5.4 Sv/yr, and for the subsurface rings 3.8 Sv/yr. Thus, even though they occur much less frequently, the subsurface rings appear to carry more than a third of the total ring-induced SAW transport. The average transport per subsurface ring is about double that of the surface rings ( $\sim 1.7$  Sv vs. 0.8 Sv). The

Table 3.

Summary of NBC Rings observed by the CM/CTD moorings.

Total number of rings:	14
Total volume transport by rings:	14.9 Sv
Average transport per ring:	1.1 Sv
Time period of observations:	20 months
Annualized ring transport:	8.9 Sv/year
Total “surface” rings:	11
Total volume transport:	9.3 Sv
Average transport per ring:	0.8 Sv
Annualized ring transport:	5.6 Sv/year
Total “subsurface” rings:	3
Total volume transport:	5.6 Sv
Average transport per ring:	1.9 Sv
Annualized ring transport:	3.3 Sv/year

Table 4.

Summary of NBC Rings observed by ship and moorings.

Total number of rings:	16
Total volume transport by rings:	16.9 Sv
Average transport per ring:	1.1 Sv
Time period of observations:	22 months*
Annualized ring transport:	9.2 Sv/year
Total “surface” rings:	12
Total volume transport:	10.0 Sv
Average Transport per ring:	0.8 Sv
Annualized ring transport:	5.4 Sv/year
Total “subsurface” rings:	4
Total volume transport:	6.9 Sv
Average transport per ring:	1.7 Sv
Annualized ring transport:	3.8 Sv/year

\* Assumes first ring shed (ship-surveyed Ring 1) passed the CM location in October 1998, and last ring shed in June 2000 (ship surveyed Ring 4) passed the CM location in July 2000.

seasonality of the SAW transport by the surface rings is investigated in Figure 11, where the SAW volume of each ring is plotted by the month in which it was formed. While there is no apparent seasonality in the formation rate of the rings, there is a distinct seasonality in the ring transport with larger SAW volumes occurring in rings that form in the late fall and early winter months. As noted previously these tend to be larger, more deeply penetrating rings, in contrast to the shallow and typically smaller rings that form in the spring and summer months. These larger rings dominate the SAW transport associated with the surface rings and account for about half of the total SAW transport by all rings. In terms of an overall classification for the rings we propose that there are three main ring types: (i) the large surface intensified rings that penetrate to depths typically greater than 400 m, (ii) the smaller surface rings that penetrate to depths less than 200 m, and (iii) the subsurface intensified rings. The corresponding percentages of the total SAW transport that these ring types account for is approximately 45%, 25%, and 30%, respectively.

### 3.4 Ring “watermass” vs. “geometric” volumes

It is useful to consider whether the SAW volumes contained in the rings can be approximated by the physical properties of the rings themselves without requiring a detailed watermass assessment of each ring, as we have done here. Oceanic rings are normally viewed as being made up of three regions, a ring interior (or core), an exterior region of mostly ambient waters, and a ring “front” that separates these two regions (Olson, 1986). In the case of rings that are formed from a mid-ocean front, such as the Gulf Stream, the ring core will contain nearly pure waters from one side of the front while the ring front will contain a mixture of waters from both sides of the front. The maximum swirl velocity will occur in this ring front region, which should be approximately aligned with the main watermass boundary. Thus the  $r_{\max}$  of the ring is a logical choice for delimiting the edge of the ring’s watermass core.

In many of the observed NBC rings there is a near correspondence between the radius of maximum velocity of the ring and the lateral boundary between the North and South Atlantic water masses. If we were to assume that the waters inside  $r_{\max}$  are made up of “pure” South Atlantic waters, and those outside of pure North Atlantic waters, then we can define a “geometric” volume for each ring which is given by the cylindrical volume  $\pi r_{\max}^2 \Delta z$ , where  $\Delta z$  is the vertical penetration (or thickness between upper and lower limits) of the ring. In reality there is mixing of North Atlantic waters into the core of the rings in some cases and also mixing of South Atlantic waters into the periphery of the rings so that this is an over-idealization of the true watermass structure of the rings. However, these effects might be expected to be largely compensatory.

The “geometric” volumes of the rings are plotted in Figure 12 against the estimated SAW volumes determined from the watermass analysis. In general,

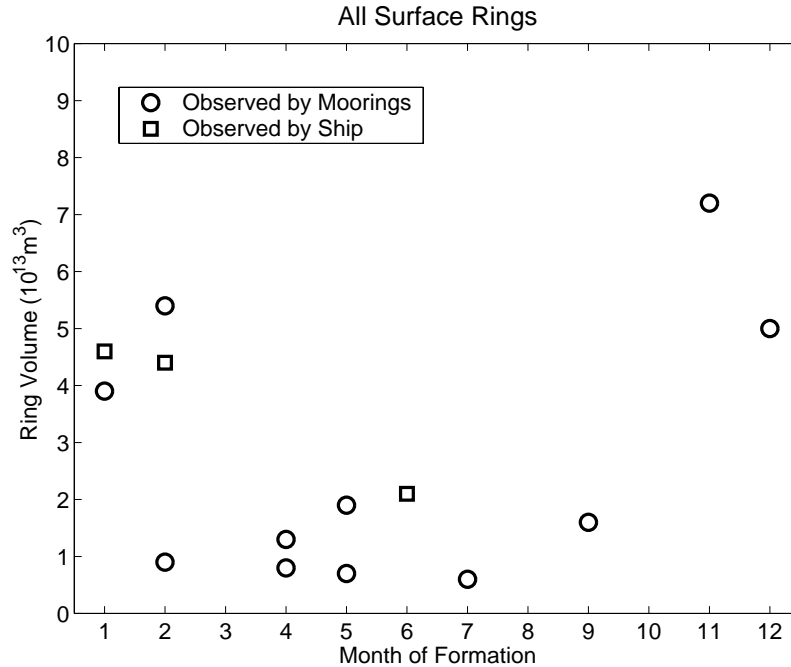


Figure 11. Annual distribution of rings formed during the experiment plotted with respect to their enclosed South Atlantic Water (SAW) volumes. The rings that form in the late fall and early winter tend to penetrate more deeply and have larger SAW volumes.

there is a good correspondence between the two estimates for the surface rings, but the watermass volumes are higher than the geometric volumes by about 15% on average. For the subsurface rings, the watermass volumes are much higher than the geometric volumes, by about a factor of two. This occurs for two reasons; first, the cores of the subsurface rings tend to have very undiluted SAW; and second, the region of relatively high SAW percentage in these features typically extends some distance beyond  $r_{\max}$ . The latter effect can be particularly significant since South Atlantic waters that occur on the periphery of the rings have a much larger associated cylindrical volumes.

The reason why the geometric volume seems to underestimate the SAW volume of the rings in general may be related to the fact that these rings are formed from a retroflecting current rather than a mid-ocean front. In the case of the NBC the waters forming the ring “front” are derived from a boundary current that is pressed up against the coast and that can only entrain ambient waters on its edges after the current separates from the coast. Therefore it should be expected that the SAW core of the rings would initially extend beyond  $r_{\max}$  before mixing effects across the ring front take effect. The actual volume of water that remains trapped within the ring circulation and is transported northward with the ring is expected to be substantially greater than the above

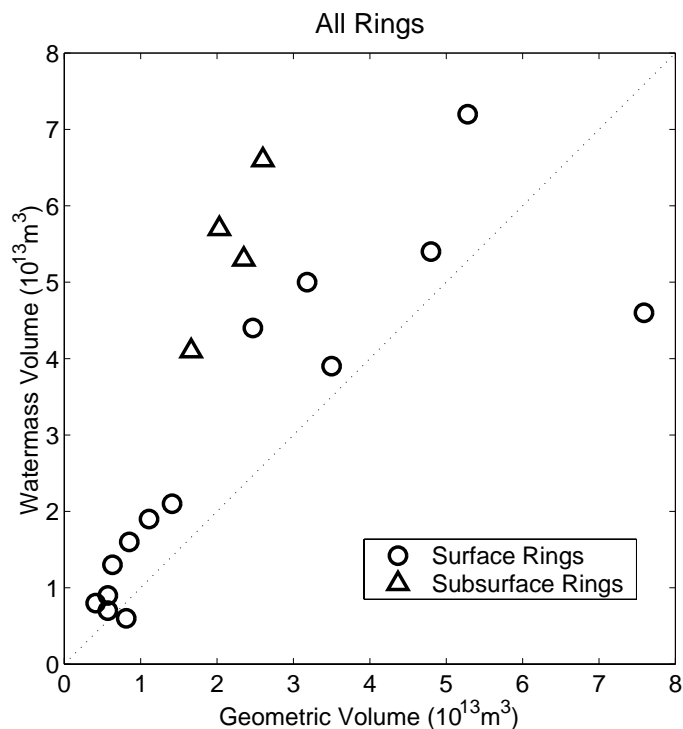


Figure 12. Comparison of calculated SAW volume for each ring and the “geometric” volume of each ring. The geometric volume is the cylindrical volume inside the radius of maximum velocity over the vertical limits of the ring.

above watermass or geometric volumes. According to Flierl (1981), the trapped volume of a ring coincides with the region where the swirl velocity magnitude exceeds the forward propagation speed of the ring, which for NBC rings is about 10-15 cm/s. Therefore, much of the ring volume, out to near the *edge radius* of the rings as we have defined it (swirl velocity > 15 cm/s), should be physically transported with the rings once they have pinched off. For the case of NBC rings, which are anticyclonic, this region would correspond to a volume that is shifted slightly shoreward relative to the center of the ring.

#### 4. DISCUSSION AND CONCLUSIONS

The purpose of this work is to assess the role played by NBC rings in the net cross-gyre transport of South Atlantic waters into the subtropical North Atlantic. It is clear from the observations that a variety of NBC ring types can occur, and that the rings can carry varying amounts of South Atlantic water. An accurate assessment of the net transport carried by the rings on a climatological basis must therefore take into account the probability of occurrence of different ring types and the representativeness of any particular observation period relative to climatology.

For the surface rings, we can assess the representativeness of our observation period against estimates of ring formation rates derived from satellite altimetry (Goni and Johns, this volume), which cover a ten year period from 1992 to 2002. The period of our observations corresponds to a relatively active period of NBC ring generation in the context of the available historical record. The ring formation rate derived from altimetry shows interannual variability ranging from a rate of 3 to 7 rings per year (Goni and Johns, their Figure 11), with our  $\sim 2$  years of observations falling among the highest formation rate found in the record. The average rate of surface ring formation derived from the altimetry record is 5 rings per year, which is less than the rate of 6.5 surface rings per year during our measurement period. This suggests that our estimate of SAW transport by the rings may be higher than the climatological value by order 30%. However, it must also be borne in mind that some rings may escape detection by altimetry. A case in point was ring R8 during the period of our experiment which was detected by the moorings and by IES but not clearly identified by altimetry. Thus it is also possible that the climatological ring formation rate derived from altimetry is low.

Another complicating factor is the large range of SAW volumes carried by the surface rings, which makes it highly nontrivial to scale the results from this experiment to a climatological ring formation rate, even if such a rate was well determined. Ideally it would be possible to distinguish between the rings that carry large volumes of SAW according to their altimetric signatures, either by their size (e.g.,  $r_{\max}$ , though this is not infallible) or by other measures such as their longevity (e.g., if more deeply penetrating rings decay more slowly), but such an understanding is not yet available. In most rings the surface swirl velocities are similar, of order 1 m/s, so that the amplitude of the SSH signal associated with a ring is not necessarily a reliable indicator. It is possible to infer (approximately) the SSH anomaly associated with the observed rings by application of a gradient momentum balance to the observed surface velocity structure across the rings; the result we obtain is that the rings have typical SSH anomalies relative to the surrounding waters of 0.15 to 0.25 m, with only marginally greater values for the larger, deep rings.

Finally, since the subsurface rings are mostly undetectable by altimetry, there is virtually no way to know how representative our observations are of the typical formation rate of these features. From our observations it appears that about two of these features are formed per year, with the times of formation occurring in the fall (September-October) and spring (March-April), although this pattern could be coincidental. At the present time we can only assume that this formation rate is representative, and that the SAW volumes we determine to be carried in these rings are also representative, despite having a sample size of only four.

An important question that arises from the discovery of these subsurface NBC rings is the dynamics that lead to their formation. One possibility is that they may form upstream of the surface NBC retroflection at the location where

the thermocline portion of the NBC (the North Brazil Undercurrent, NBUC; Schott *et al.*, 1998) retroflects into the Equatorial Undercurrent (EUC). This could explain the subsurface-intensified nature of these features, but cannot explain why they usually have a thick layer of SAW extending down to intermediate water levels, nor why some of these features have swirl velocity maxima at depths of 600-800 m, which is far below the core level of the EUC (~150 m). Another hypothesis for their generation is that they are the result of an instability process of an intermediate depth current (the Intermediate Western Boundary Current; IWBC) that breaks up into eddies as it crosses the equator (Jochum and Malanotte-Rizzoli, 2003). This could lead to the observed structure of some of these features, but as yet there is not any observational evidence to confirm that such a process is taking place.

An equally important question is: Why are two distinct classes of surface-intensified rings formed, and why do the deep-reaching rings with large SAW volumes preferentially form in the late fall to early winter? The answer likely has to do with the seasonal cycle of the NBC and its retroflection into the NECC. The NBC reaches its maximum strength during August-September, and decreases to minimum strength in April-May (Johns *et al.*, 1998). The NBC retroflection is present from about June to March and is either weak or absent during the period of minimum NBC transport in April-May. The large, deep-reaching rings seem to be formed during the period when the NBC is in its declining phase from the summer transport maximum, but while the NBC retroflection is still clearly established. At this time of year the NBC also has a deep reaching flow structure that extends to depths of 800 m, which could explain the formation of deep-reaching rings at this time. In contrast, during spring and early summer the NBC flow is mostly confined to the surface layers above 150 m (Johns *et al.*, 1998), which is consistent with the shallow rings that form at this time of year. A remaining puzzle is the manner in which these shallow rings are formed, since at least some of them form when the retroflection is not clearly established. This suggests a different formation mechanism than the canonical retroflection pinch-off process that occurs during the time when the retroflection is established. The mechanism of the formation of these shallow features requires further investigation.

An encouraging development in the study of NBC rings is the emergence of several new basin scale numerical simulations and idealized regional models that exhibit vigorous NBC ring shedding behavior, and that appear to have many similarities to the observed phenomenology of NBC rings (Barnier *et al.*, 2001; Garraffo *et al.*, this volume; Jochum and Malanotte-Rizzoli, 2003). The results described in Garraffo *et al.* (this volume) in particular, based on a high-resolution Atlantic MICOM (Miami Isopycnal coordinate model) simulation, bear a remarkable resemblance to the observations in terms of the number of rings shed, the generation of different ring types (including subsurface-intensified rings), and the volumes of South Atlantic waters transported by the rings. Using a watermass analysis similar to that performed here, Garraffo *et al.*

obtain a mean ring-induced transport of 7.5 Sv over 6 years of their model simulation, with a range from 5.5 to 9.0 Sv in individual model years. Interestingly, the Garraffo *et al.* results are obtained from a climatologically forced model, which suggests that there may be natural variability in the ring formation rate and its associated cross-gyre transport regardless of variability caused by interannual forcing.

In summary, we find from these new observations that NBC rings form an important part of the net meridional transport of South Atlantic waters from the equatorial to subtropical North Atlantic ocean, and that their contribution to this transport has probably been underestimated by previous studies. The annualized rate of South Atlantic water transport by the rings during the period of our experiment, from October 1998 to June 2000, was approximately 9 Sv, which amounts to more than half of the estimated rate of upper ocean transport in the MOC of 13-17 Sv (Schmitz and Richardson, 1991; Roemmich and Wunsch, 1985). Other important pathways may include seasonal interior transport associated with the storage of southern hemisphere waters in the NECC and subsequent northward transport in the Ekman layer (Mayer and Weisberg, 1993), and residual coastal flow near the western boundary that is not associated with rings. In contrast to previous conclusions, however, the results of our analysis suggest that NBC rings may in fact be the dominant pathway. The results of this experiment also serve to illustrate the point that remote sensing of NBC rings by satellite altimetry or ocean color will not be sufficient to adequately determine the cross-gyre transport carried by NBC rings, due to the great variability in vertical structures of the rings. A combination of remote sensing observations and *in-situ* time series that can observe the vertical structures of the rings, such as provided here by the moorings, is proposed as a possible strategy for longer term monitoring of the NBC rings and their cross-gyre transport.

### **Acknowledgements**

This research was supported by the U.S. National Science Foundation under grant number OCE-9730322, and in part by NOAA/AOML (G.G.). We express our gratitude to the captain and crew of the R/V Seward Johnson for their able assistance in the deployment and recovery of the moored instruments and the shipboard survey work during the four project cruises. S. Garzoli kindly provided estimates of the NBC ring translation speeds from the IES array. The authors would like to thank D. Olson, Z. Garraffo, and E. Johns for helpful scientific discussions.

## REFERENCES

- Barnier, B., T. Reynaud, A. Beckmann, C. Boning, J-M Molines, S. Barnard, Y. Jia, On the seasonal variability and eddies in the North Brazil Current: Insight from model intercomparison experiments. *Prog. Oceanogr.*, **44**, 195-230, 2001.
- Bourles, B., R.L. Molinari, E. Johns, W.D. Wilson, and K.D. Leaman, Upper layer currents in the western tropical North Atlantic (1989-1991). *J. Geophys. Res.*, **104**, 8555-8560, 1998.
- Didden, N. and F. Schott, Eddies in the North Brazil Current retroflection region observed by Geosat altimetry. *J. Geophys. Res.*, **98**, 20121-20131, 1993.
- Emery, W.J., and J.S. Dewar, Mean Temperature-Salinity, Salinity-Depth, and Temperature-Depth curves for the North Atlantic and North Pacific. *Prog. Oceanogr.*, 11219-11305, 1982.
- Fleurant, C., D. Wilson, W. Johns, S. Garzoli, R. Smith, D. Fratantoni, P. Richardson and G. Goni. CTD02, LADCP and XBT measurements collected aboard the R/V Seward Johnson, February–March 1999 North Brazil Current Rings Experiment Cruise 2 (NBC02). NOAA Data Report OAR AOML-37, 2000.
- Fleurant, C., D. Wilson, W. Johns, S. Garzoli, R. Smith, D. Fratantoni, P. Richardson and G. Goni. CTD02, LADCP and XBT measurements collected aboard the R/V Seward Johnson, December 1998 North Brazil Current Rings Experiment Cruise 3 (NBC3). NOAA Data Report OAR AOML-38, 2000.
- Flierl, G.R., Particle motions in large amplitude wave fields. *Geophys. Astro. Dyn.*, **18**, 39-74, 1981.
- Fratantoni, D.M., W.E. Johns, T.L. Townsend, Rings of the North Brazil Current: their structure and behavior inferred from observations and a numerical simulation. *J. Geophys. Res.*, **C6**, 10,633-10,654, 1995.
- Fratantoni, D.M. and D. Glickson, North Brazil Current ring generation and evolution observed with SeaWiFS, *J. Phys. Oceanogr.*, 2002.
- Garzoli, S.L., A. Ffield, W.E. Johns, and Q. Yao. North Brazil Current retroflection and transports. *J. Mar. Res.*, 2003.
- Goni, G.J., and W.E. Johns, A census of North Brazil Current rings observed from TOPEX/Poseidon altimetry: 1992-1998. *Geophys. Res. Lett.*, **28**, 1-4, 2001
- Johns, W.E., T.N. Lee, F.A. Schott, R.J. Zantopp, R.H. Evans, The North Brazil Current retroflection: Seasonal structure and eddy variability. *J. Geophys. Res.*, **95** (C12), 22,103-22,120, 1990.
- Johns, W.E., T.N. Lee, R.C. Beardsley, J. Candela, R. Limeburner and B. Castro, Annual cycle and variability of the North Brazil Current. *J. Phys. Oceanogr.*, **28**, 103-128, 1998.
- Jochum, M. and P. Malanotte-Rizzoli, On the generation and importance of North Brazil Current rings. *J. Mar. Res.*, **61**, 147-162, 2003.
- Levitus, S., Climatological Atlas of the World Ocean, . NOAA Professional Paper 13, US Dept of Commerce, NOAA, 1982.

- Mayer, D.A and R.H. Weisberg, A description of COADS surface meteorological fields and the implied Sverdrup transports for the Atlantic Ocean from 30°S to 60°N. *J. Phys. Oceanogr.*, **23**, 2201-2221, 1993.
- Olson, D.B., Lateral exchange within Gulf stream warm-core ring surface layers. *Deep-Sea Res.*, **33**, Nos.11/12, 1691-1704. 1986.
- Richardson, P.L., G.E. Hufford, R. Limeburner, and W.S. Brown, North Brazil Current retroflection eddies. *J. Geophys. Res.*, **99**(C3), 5081-5093, 1994.
- Roemmich, D., and C. Wunsch, Two transatlantic sections: Meridional circulation and heat flux in the subtropical North Atlantic Ocean. *Deep-Sea Res.*, **32**, 609-664, 1985.
- Schmitz, W. Jr., and P. Richardson, On the sources of the Florida Current. *Deep-Sea Res.*, **38**, Suppl., S379-S409, 1991.
- Schott, F.A., J. Fischer, L. Stramma, Transports and pathways of the Upper-layer circulation in the western tropical Atlantic. *J. Phys. Oceanogr.*, **28**, 1904-1928, 1998.
- Wilson, W.D., E. Johns, and R. L. Molinari, Upper layer circulation in the western tropical North Atlantic during August 1989. *J. Geophys. Res.*, **99**, 22,513-22,523, 1994.
- Wilson, D. W., W. Johns and S. L. Garzoli. Velocity structure of North Brazil Current rings. *Geophys. Res. Lett.*, **29**, 10.1029/2001GL013869, 2001.
- Wüst, G., Stratification and Circulation in the Antillean-Caribbean Basin. Columbia University Press, New York, 201 pp., 1964.